An Interactive Shader for Natural Diffraction Gratings

Bachelorarbeit

der Philosophisch-naturwissenschaftlichen Fakultät
der Universität Bern

vorgelegt von

Michael Single

2014

Leiter der Arbeit:
Prof. Dr. Matthias Zwicker
Institut für Informatik und angewandte Mathematik

Abstract

In nature, animals exhibit structural colors because of the physical interaction of light with the nanostructures of their skin. In his pioneering work, J.Stam developed a reflectance model based on wave optics capturing the effect of diffraction from surface nanostructures. His model is dependent on an accurate estimate of the correlation function using statistical properties of the surface's height field. We propose an adaption of his BRDF model that can handle complex natural gratings directly. Furthermore, we describe a method for interactive rendering of diffraction effects due to interaction of light with biological nanostructures such as those on snake skins. Our method uses discrete height fields of natural gratings acquired by using atomic force microscopy (AFM) as an input and employs Fourier Optics to simulate far-field diffraction. Based on a Taylor Series approximation for the phase shifts at the nanoscale surface, we leverage the precomputation of the discrete Fourier Transformations involved in our model, to achieve interactive rendering speed (about 5-15 fps). We demonstrate results of our approach using surface nanostructures of two snake species, namely the *Elaphe* and the *Xenopeltis* species, when applied to a measured snake geometry. Lastly, we evaluate the quality of our method by comparing its (peak) viewing angles with maximum reflectance for a fixed incident beam with those resulting from the grating equation at different wavelengths. We conclude that our method produces accurate results for complex, natural gratings at interactive speed.

Contents

Chapter 1

Theoretical Background

1.1 Basics in Modelling Light in Computer Graphics

1.1.1 Radiometry

One purpose of Computer Graphics is to simulate the interaction of light with a surface and how a real-world observer, such as a human eye, will perceive this. These visual sensations of an eye are modelled relying on a virtual camera which captures the emitted light from the surface. The physical basis to measure such reflected light is studied under radiometry which deals with measures on the electromagnetic radiation transferred from a source to a receiver.

Fundamentally, light is a form of energy propagation, consisting of a large collection of photons, whereat each photon can be considered as a quantum of light that has a position, a direction of propagation and a wavelength λ. A photon travels at a certain speed $v = c/n$, that depends only the speed of light c and the refractive index n through which it propagates. Its frequency is defined by $f = v/\lambda$ and its carried amount of energy q, measured in the SI unit Joule, is given by $q = hf = hv/\lambda n$ where h is the Plank's constant. The total energy of a large collection of photons is hence $Q = \sum_i q_i$.

1.1.2 Spectral Energy

It is important to understand that the human eye is not equally sensitive to all wavelength of the spectrum of light and therefore responds differently to specific wavelengths. Remember that our goal is to model the human visual perception. This is why we consider the energy distribution of a light spectrum rather than considering the total energy of a photon collection since then we could weight the distribution according to the human visual system. So the question we want to answer is: How is the energy distributed across wavelengths of light?

One idea is to make an energy histogram from a given photon collection. For this we have to order all photons by their associated wavelength, discretize the wavelength spectrum, count all photons which then will fall in same wavelength-interval, and then, finally, normalize each interval by the total energy Q. This will give us a histogram which tells us the spectral energy Q_λ for a given discrete λ interval and thus models the so called spectral energy distribution [1].

[1] Intensive quantities can be thought of as density functions that tell the density of an extensive quantity at an infinitesimal by a small interval or a point.

1.1.3 Spectral Power

Rendering an image in Computer Graphics corresponds to capturing the color sensation of an illuminated, target scene at a certain point in time. each color is associated with a wavelength and is directly related to a certain amount of energy. In order to determine the color of a to-be-rendered pixel of an image, we have to first get a sense of how much light (in terms of energy) passes through the area which the pixel corresponds to. We begin by considering the flow of energy $\Phi = \frac{\Delta Q}{\Delta t}$ transferred through this area over a unit period of time. This allows us to measure the energy flow through a pixel during a certain amount of time. In general, power is the estimated rate of energy production for light sources and corresponds to the flux. It is measured in the unit Watts, denoted by Q. Since power is a rate over time, it is well defined even when energy production is varying over time. As with Spectral Energy for rendering, we are really interested in the spectral power $\Phi_\lambda = \frac{\Delta\Phi}{\Delta\lambda}$, measured in Watts per nanometer.

1.1.4 Spectral Irradiance

Before we can tell how much light is reflected from a given point on a surface towards the viewing direction of an observer, we first have to know how much light arrives at this point. Since in general a point has no length, area or even volume associated, let us instead consider an infinitesimal area ΔA around a such a point. Then, we can ask ourself how much light falls in such a small area. Further while observing this process over a short period of time, the measured quantity gives us the the spectral irradiance E as illustrated in figure 1.1. Summarized, this quantity tells us how much spectral power is incident on a surface per unit area and mathematically is equal:

$$E_\lambda = \frac{\Phi_\lambda}{\Delta A} \tag{1.1}$$

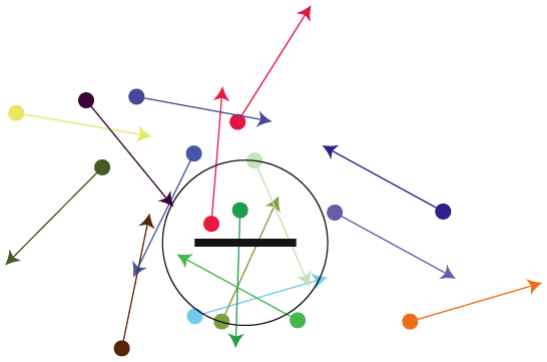

Figure 1.1: Irradiance is the summed up radiance over all directions. The black border is representing a surface element.

1.1.5 Spectral Radiance

When rendering an image we have to determine the color of each pixel of the image. Although irradiance tells us how much light is arriving at a point and gets reflected, it tells us nothing about the power distribution across different directions. The direction of the element is important because the human eye may perceive the brightness of an illuminated objects differently when looking from direction.

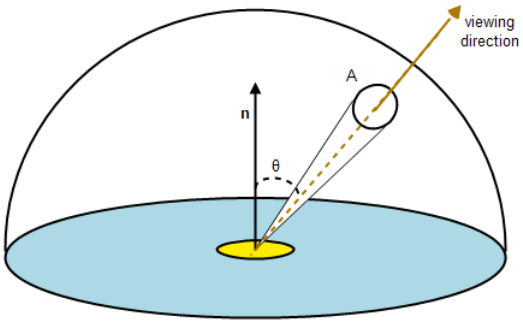

(a) Radiances is the density of photons per area per solid angle

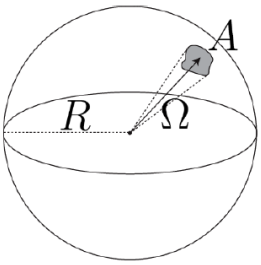

(b) Solid angle is the area of a surface patch on a sphere with radius R which is spanned by a set of directions

This concept is described by the radiometric quantity radiance. Basically, radiance is the measure of light energy passing through or emitted from a small area around a point on a surface towards a given direction during a short period in time. More formally this is the spectral power emerging from an arbitrary point (an infinitesimal area around this point) and falls within a given solid angle (see figure[2] 1.2(b)) in a specific direction (usually towards the observer) as shown in figure 1.2(a). Formally, this leads us to the following mathematical formalism:

$$L_\lambda(\omega) = \frac{d^2\Phi_\lambda}{dAd\Omega} \approx \frac{\Phi_\lambda}{\Omega A} \tag{1.2}$$

where L is the observed spectral radiance in $Wm^{-}2sr^{-}1$ in direction ω, Θ_λ is the total power emitted, θ is the angle between the surface normal and the specified direction, A is the area of the surface and Ω is the solid angle subtended by the observation or measurement.

It is useful to distinguish between radiance incident at a point on a surface and excitant from that point. Terms for these concepts sometimes used in the graphics literature are surface radiance L_r for the radiance *reflected* from a surface and field radiance L_i for the radiance *incident* at a surface.

1.1.6 BRDF

In order to render the colorization of an observed object, a natural question in Computer Graphics is what portion of the incident light a viewer will receive after reflection, after when he looks at an illuminated object. For any given surface which is illuminated from a certain direction ω_i, we can ask ourself how much light is reflected from any point on this surface towards a viewing direction ω_r. This is where the Bidirectional Reflectance Distribution Function (BRDF) comes into play, which is a radiometric quantity telling us how much light is reflected at an opaque surface. Mathematically speaking, the BRDF is the ratio of the reflected radiance pointing in the direction ω_r to the incident irradiance coming from the inverse direction of ω_i as illustrated in figure 1.2. Hence the BRDF is a four dimensional function defined by four angles θ_i, ϕ_i, θ_r and ϕ_r.

Formally, a BRDF for any given wavelength λ is defined as:

[2]Modified from a figure in Computer Graphics class 2012 in chapter *Colors*

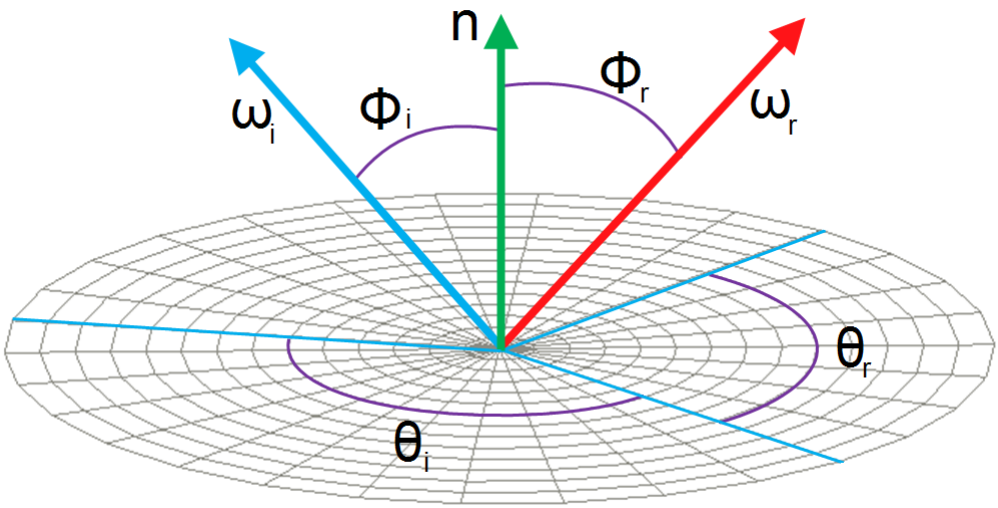

Figure 1.2: Illustration of the BRDF model, where ω_i is pointing to the light source and the viewing direction is denoted by ω_r. Both unit direction vectors are defined w.r.t to a surface normal **n** for every point on the surface.

$$BRDF_\lambda(\omega_i, \omega_r) = \frac{dL_r(\omega_r)}{dE_i(\omega_i)} = \frac{dL_r(\omega_r)}{L_i(\omega_i)cos(\theta_i)d\omega_i} \tag{1.3}$$

Where L_r is the reflected spectral radiance, E_i is the incident spectral irradiance and θ_i is the angle between ω_i and the surface normal **n**. Also, L_i is the incident spectral radiance.

1.1.7 Wavespectrum and Colors

In order to see how crucial the role of human vision plays, let us consider the following definition of color by *Wyszechkiu and Siles*[3] stating that *"Color is the aspect of visual perception by which an observer may distinguish differences between two structure-free fields of view of the same size and shape such as may be caused by differences in the spectral composition of the radiant energy concerned in the observation"*. Therefore, similarly like the humans' perceived sensation of smell and taste, color vision is just another individual sense of perception giving us the ability to distinguish between different frequency distributions of light which we experienced as different colors.

[3]mentioned in Computer Graphics Fundamentals Book from the year 2000

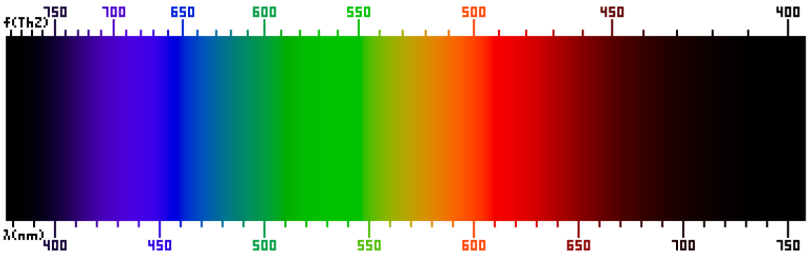

Figure 1.3: Frequency (top) and wavelength (bottom) of colors of the visible light spectrum[4].

In general, an eye consists of photoreceptor cells which are responsible for providing ability of color-perception. A schematic of an eye is illustrated in figure 1.4. Basically, there are two specialized types of photoreceptor cells, cone cells which are responsible for color vision and rod cells, which allow an eye to perceive different brightness levels.

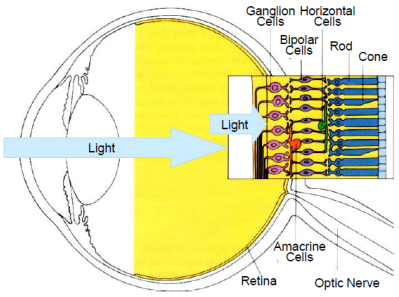

Figure 1.4: Schematic[5] of photoreceptor cells, cones and rods, in a human eye

A human eye is made of three different types of cone cells, having their peak sensitivity in different wavelength ranges. More precisely, there are cone cells most sensitive to short wavelengths between $420nm$ and $440nm$, those which are most sensitive in the middle range between $530nm$ and $550nm$ and those which have their peak in the long range, from $560nm$ to $580nm$. Therefore, any color sensation in human color perception can therefore be described by just three parameters, corresponding to the levels of stimulus of these three types of cone cells.

1.1.8 Colorspace

In order to render accurate images of how a human observer sees its world, a mathematical model of the human color perception is required. Remember that color sensation is due to a visual stimulus processed by cone cells in an eye. A human eye contains three different types of cone cells. Therefore, one possible approach is to describe each kind of these cone cells with a function mapping each wavelength to a certain sensitivity. In the early 1920 from a series of experiments, the so called CIE RGB color space was derived. This space describes the response of cone cells of an average human individual, the so called standard observer. Basically, a statistically sufficiently large number of probands were exposed to different target light colors expressed by their wavelength. The task of each proband was to reproduce these target colors by mixing three given primary colors, red, green and blue light. The strength of each primary color could be manually adjusted by

[4]Similar figure like used in computer graphics class 2012 in chapter colors
[5]image of illustration has been taken from `http://en.wikipedia.org/wiki/Bidirectional_reflectance_distribution_function`

setting their relative sensitivity. Those adjustment weights have been measured, aggregated and averaged among all probands for each primary color. This model describes each color as a triple of three real valued numbers[6], the so called tristimulus values. Summarized, these experiments provided certain weights of primary colors in order to match a color at a certain wavelength according to the average human color perception. However, some of these weights could have a negative value.

The disadvantage of the CIE RGB colorspace is that some of its color weights are negative. Thus, scientist dervied the CIE XYZ colorspace which as no negative color matching functions but is still additive[7]. Figure 1.5 visualizes the matching functions of the CIE XYZ space. Another property of the CIE XYZ space is that its Y component is representing the luminance of the corresponding color. Usually, the CIE XYZ space is used as a reference colorspace to define colorspace transformations.

Pragmatically speaking, color spaces describe the range of colors a camera can see, a printer can print or a monitor can display. Thus, formally we can define it as a mapping from a range of physically produced colors from mixed light to a standard objective description of color sensations registered in the eye of an observer in terms of tristimulus values.

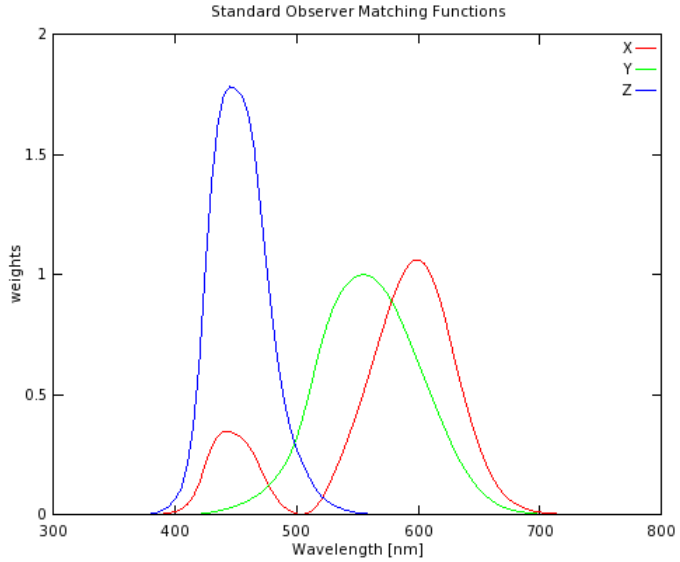

Figure 1.5: Plots of our color matching functions we used for rendering

Interpolating all measured tristimuli values gives us three basis functions, the CIE color matching functions $\overline{x}(\lambda), \overline{y}(\lambda), \overline{z}(\lambda)$. In figure 1.5 are the numerical description of the chromatic response of the observer. They can be thought of as the spectral sensitivity curves of three linear light de-

[6]note that there are negative color weights possible in the CIE RGB colors space. This is why some human perceived color sensations could not be reconstructed using just an additive color model (adding three positively weighted primary values). Therefore, a probabant was also allowed to move one of the primary colors to the target color and instead was supposed to reproduce this new color mix using the two remaining primaries (subtractive model). The value of the selected, moved primary was then interpreted as being negative weighted in an additive color model.

[7]Remember, the property of an additive colorspace is that any color can be represented as a weighted sum of matching functions of that color space.

tectors yielding the CIE tristimulus values X, Y and Z.

The tristimulus values for a color with a spectral power distribution $I(\lambda)$, are given in terms of the standard observer by:

$$\begin{aligned} X &= \int_{\Lambda} I(\lambda)\,\overline{x}(\lambda)\,d\lambda \\ Y &= \int_{\Lambda} I(\lambda)\,\overline{y}(\lambda)\,d\lambda \\ Z &= \int_{\Lambda} I(\lambda)\,\overline{z}(\lambda)\,d\lambda \end{aligned} \tag{1.4}$$

where λ is the wavelength of the equivalent monochromatic light spectrum $\Lambda = [380nm, 780nm]$. Note that it is not possible to build a display that corresponds to the CIE XYZ colorspace. For this reason it is necessary to design other color spaces, which are physically realizable, efficiently encoded, perceptually uniform and have an intuitive color specification. There are simple conversions between XYZ color spaces to other color space - such as the RGB colorspace - described as linear transformations.

1.1.9 Spectral Rendering

When rendering an image, most of the time we are using colors described in a certain RGB color space. However, a RGB colorspace results from a colorspace transformation of the tristimulus values, which themselves are inherent to the human visual system. Therefore, many physical phenomenon are poorly modelled when they rely on RGB colors for rendering. Using only RGB colors for rendering is like assuming that a given light source emits light of only three particular wavelengths. But in reality this is rarely the case. Spectral rendering refers to using certain wavelength spectrum, for e.g. the human visible light spectrum, instead of simply using only the range of RGB values in order to render an illuminated scene. This captures the physical reality of specific light sources way more accuratly. Keep in mind that even when we make use of a spectral rendering approach, we have to convert the final spectra to RGB color values when we want to display an image on an actual display.

1.2 Wave Theory for Light and Diffraction

1.2.1 Basics in Wave Theory

In order to prepare the reader for relevant concepts in physics which are used later for derivations and reasonings within this thesis, I am going to provide a quick introduction to the basics of wave theory and related concepts. In physics, a wave describes a disturbance that travels from one location to another through a certain medium. The disturbance temporarily displaces the particles in the medium from their rest position which results in an energy transport along the medium during wave propagation. Usually, when talking about waves we are actually referring to a complex valued function which is a solution to the so called *wave equation* which is modelling how the wave disturbance proceeds in space during time.

There are two types of waves, (a) mechanical waves which deform their mediums during propagation like sound waves and (b) electromagnetic waves consisting of periodic oscillations of an

electromagnetic field, such as light. As illustrated in figure 1.6, there are several properties someone can use and apply in order to compare and distinguish different waves:

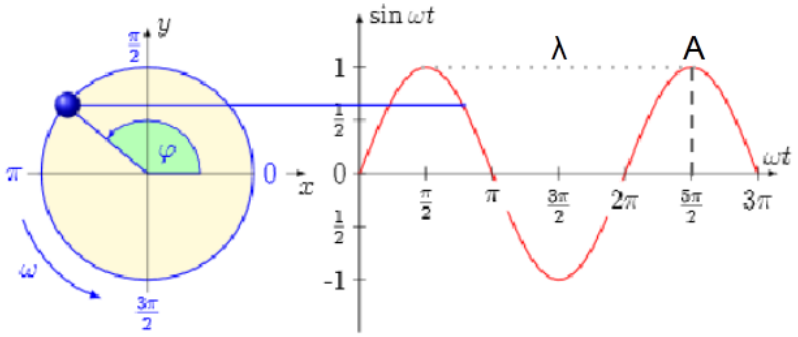

Figure 1.6: Simplified, one dimensionally real valued wave function[8], giving an idea about some important wave properties. We denote the crest of a wave as the highest point relative to the equilibrium line (zero height along time axis) and similarly the trough as the lowest point.

Wavelength: It ss usually denoted by λ and is a measure for the spatial distance from one point to another until the shape of a wave repeats

Amplitude: It is denoted by A and there are two possible interpretations: Firstly, it is a measure of the height from the equilibrium point to the highest point of a crest on the wave or the lowest point of a trough. This means that the amplitude can be positive or negative. However, usually, someone is just interested in the absolute value of an amplitude, i.e. the magnitude of a wave. For light waves it is a relative measure of intensity or brightness to other light waves of the same wavelength. And secondly, it can be interpreted as a measure how much energy a wave carries whereat the greater the absolute amplitude value, the bigger the amount of energy being carried.

Frequency: Is a measure of the number of waves which are passing through a particular point in the propagation medium during one unit of time and is denoted by f.

Phase: It is denoted by φ. It describes either the offset of initial position of a wave or the relative displacement between or among waves having the same frequency. Two waves two waves with same frequency are said to be in phase if they have the same phase. This means that they line up everywhere. As a remark, we denote by ω the angular frequency which is equal $2\pi f$.

A geometrical property of waves is their wavefront. This is either a surface or line along the path of wave propagation on which the disturbance at every point has the same phase. Basically, a wavefront can have any kind of shape although three prominent types of wavefronts are: spherical-, cylindrical- and plane wavefronts. If a point in an isotropic medium is sending out waves in three dimensions, then the corresponding wavefronts are spheres, centered on the source point. Hence spherical wavefront is the result of a spherical wave, also denoted as a wavelet. Note that for electromagnetic waves, the phase is a position of a point in time on a wavefront cycle (motion of wave over a whole wavelength) whereat a complete cycle is defined as being equal to $360°$.

[8]Image source: http://neutrino.ethz.ch/Vorlesung/FS2013/index.php/vorlesungsskript

1.2.2 Wave Interference

Next, after having seen that a wave is simply a traveling disturbance along a medium, having some special properties, someone could ask what happens when there are several waves traveling on the same medium. Especially, we are interested in how these waves will interact with each other. In physics the term interference denotes the interaction of waves when they encounter each other at a point along their propagation medium. At each point where two waves superpose, their total displacement is the sum of the displacements of each individual wave at that point. Then, the resulting wave is having a greater or lower amplitude than each separate wave and we can interpret the interference as the addition operates on waves. Two extreme scenarios are illustrated in figure 1.7 for waves with same frequency and equal amplitude. There are basically three variants of interferences which can occur, depending on how crest and troughs of the waves are matched up:

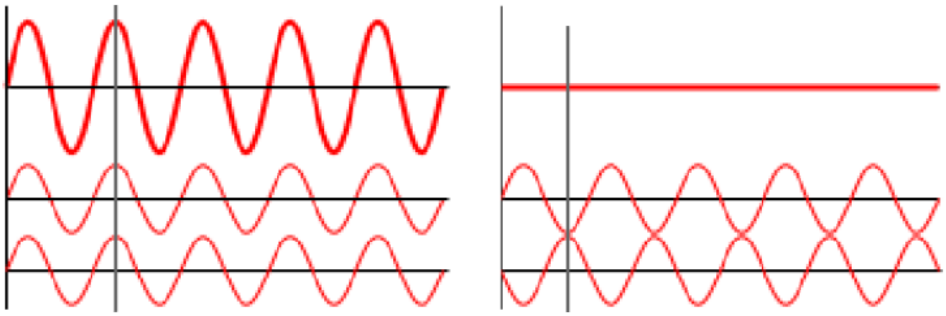

Figure 1.7: Interference scenarios[9] when two waves waves meet: On the left hand-side, there is constructive interference and on the right hand-side there is destructive interference illustrated.

- A crest of a wave meets a crest of another wave and similarly a trough meets a trough of another wave. This scenario is denoted as constructive interference and occurs at any location along the medium where the two interfering waves have a displacement in the same direction. This is like saying that the phase difference between the waves is a multiple of 2π. Then the resulting amplitude at that point is being much larger than the amplitude of an individual wave. For two waves with an equal amplitude interfering constructively, the resulting amplitude is twice as large as the amplitude of an individual wave.
- A crest of a wave meets a trough of another wave and vice versa. This scenario is denoted as destructive interference and occurs at any location along the medium where the two interfering waves have a displacement in the opposite direction. This is like saying that the phase difference between the waves is an odd multiple of π. Then the waves completely cancel each other out at any point they superimpose.
- If the phase difference between two waves is intermediate between the first two scenarios, then the magnitude of the displacement lies between the minimal and maximal values which we could get from constructive interference.

Keep in mind that when two or more waves interfere which each other, the resulting wave will have a different frequency. For a wave, having a different frequency also means having a different wavelength. Therefore, this directly implies that a light of a different color, than its source waves have, is emitted.

[9] Image source: `http://en.wikipedia.org/wiki/Interference_(wave_propagation)`

1.2.3 Wave Coherence

When considering waves which are traveling on a shared medium along the same direction, we could examine how their phase difference is changing over time. Formulating the change in their relative phase as a function of time will provide us a quantitative measure of the synchronization between those two waves, the so called wave coherence. In order to better understand this concept, let us consider a perfectly mathematical sine wave and a second wave which is a phase-shifted replica of the first one. A property of these mathematical waves is that they keep their shape over an infinity amount of time (i.e. propagated wavelengths). In our scenario, both waves are traveling along the same direction on the same medium, as illustrated in figure 1.8.

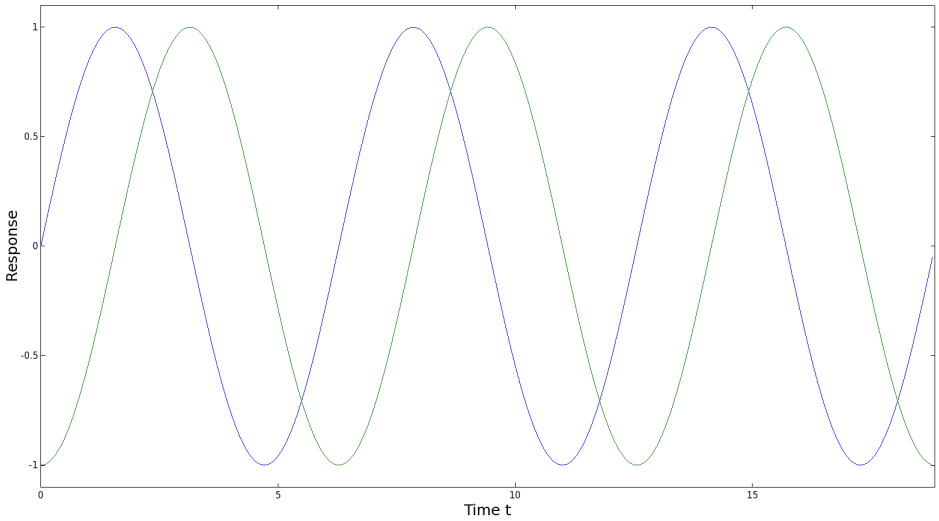

Figure 1.8: Two mathematical sine waves which are perfectly coherent which means that their phase difference is constant for every point in time.

Taking the difference between these two sine waves always yields a constant number. Therefore, those two waves are said to be coherent and hence perfectly synchronous over time. Notice that this scenario is completely artificial since in nature there are no mathematical sine waves. Rather, the phase difference is then a function of time $p(t)$. The more coherent two waves are, the slower this function will change over time. In fact, two waves are said to be coherent if they are of the same frequency, are temporally in phase or have the same amplitude at every point in time. Thus two waves are coherent if they are generated at the same time, having the same frequency, amplitude, and phase. Conversely, waves are considered incoherent or also asynchronous if they have no stable phase difference. This means $p(t)$ is heavily varying over time. Coherence describes the effect of whether waves will tend to interfere with each other constructively or destructively at a certain point in time and space. Thus this is a property of waves that enables stationary interference. The more correlated two waves are, the higher their degree of coherence is. In physics coherence between waves is quantified by the cross-correlation function, which basically predicts the value of a second wave using the value of the first one. There are two basic coherence classifications:

- Spatial coherence is dealing with the question of what is the range of distance between two points in space in the span of a wave for which there is occurring a significant effect of stationary interference when averaged over time. This is formally answered by considering the

correlation between waves at different point in space. The range of distance with significant coherence is also denoted as the coherence area.

- Temporal coherence examines how well two waves which are observed at two different moments in time correlate with each other. Thus it may be used for predicting how well a wave interferes temporally with itself. Mathematically, this kind of coherence is computed by measuring the correlation between the value of the wave and the delayed version of itself. The coherence time denotes the maximum time delay for which the waves are coherent. The distance a wave has traveled during the coherence time is denoted as their temporal coherence length.

1.2.4 Huygen's Principle

Besides the phases and the amplitudes of waves, their propagation directly affects the interaction between different waves and how they could interfere with each other. This is why it makes sense to formulate a model which allows us to predict the position of a moving wavefront and how it moves in space. This is where *Huygen's Principle* comes into play. It states that any point of a wavefront may be regarded as a point source that emits spherical wavelets in every direction. Within the same propagation medium, these wavelets travel at the same speed as their source wavefront. The position of the new wavefront results by superimposing all of these emitted wavelets. Geometrically, the surface that is tangential to the secondary waves can be used in order to determine the future position of the wavefront. Therefore, the new wavefront encloses all emitted wavelets. Figure 1.9 visualizes Huygen's principle for a wavefront reflected off from a plane surface.

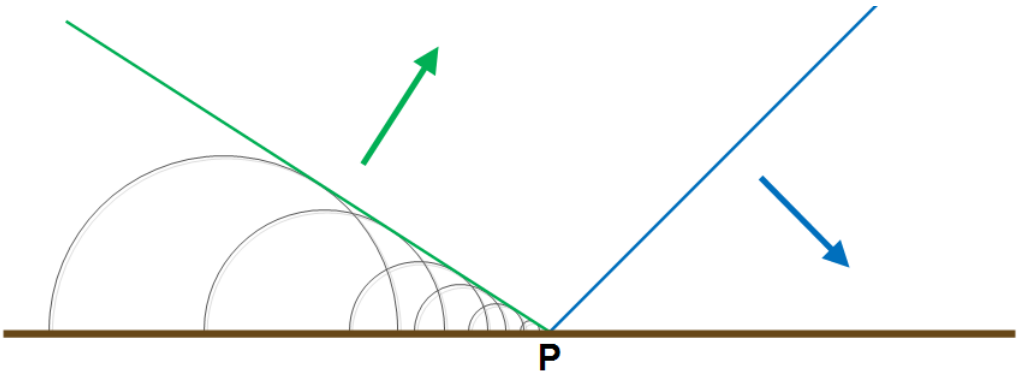

Figure 1.9: A moving wavefront (blue) encounters an obstacle (a surface shown in brown colors) and produces a new wavefront (green) as a result of superposition of all secondary wavelets.

1.2.5 Waves Diffraction

Revisting Hugen's Principle we know that each point on a wavefront can be considered as a source of a spherical wavelet which propagates in every direction. But what exactly happens when a wave's propagation direction is only partially occluded by an object? What will be the outcome on applying Huygen's Principle to this case? An example scenario for this case is shown in figure 1.10.

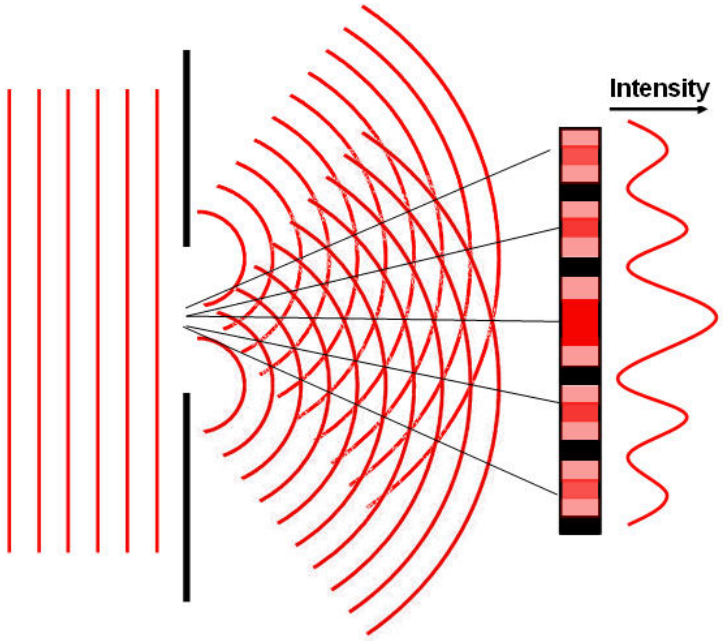

Figure 1.10: Illustration[10] of a diffraction scenario in which a plane wavefront passes through a surface with a certain width and how the wave will be bent, also showing the intensity of the resulting wave along a straight line in its path.

Whenever a propagating wavefront is partially occluded by an obstacle, the wave is not only moving in the direction along its propagation, but is also bent around the edges of the obstacle. In physics, this phenomenon is called diffraction. Waves are diffracted due to interference which occurs among all wavelets when applying Huygen's Principle for the case when a wavefront hits an obstacle. Generally, the effect of diffraction is most pronounced for the waves whose wavelength is roughly similar in size to the dimension of the occluding object. Conversely, if the wavelength is much smaller in size, then there is almost no wave diffraction perceivable at a far off distance. This relationship between the strength of wave diffraction and the wavelength is conceptually illustrated in figure 1.11 when a wave is transmitted through an opening in a surface. A reflective example for diffraction provided in figure 1.9.

[10]Image source:`http://cronodon.com/images/Single_slit_diffraction_2b.jpg`

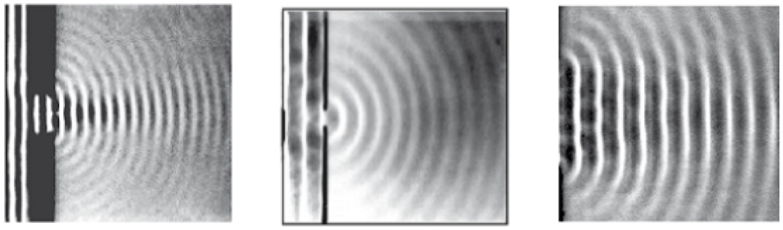

(a) W $\ll \lambda$ (b) W $\approx 2\lambda$ (c) W $\approx 6\lambda$

Figure 1.11: Illustration[11] of how diffraction changes when a wave with wavelength λ propagates through a slit of width equal W.

In everyday's life, we can see the direct outcome of the effect of wave diffraction in form of structural colors. There are examples from nature such as the iridescent colors on various snake skins as well as artificial examples such as the colorful patterns notable when having a close look at an illuminated compact disc. All these examples comprise a surface made of highly regular nanostructures which diffract an incident light significantly. Such a nanostructure which exhibits a certain degree of regularity is also denoted as a diffraction grating. Further information about diffraction gratings can be found in section **??**.

1.3 Stam's BRDF formulation

The theoretical foundation of this thesis is based on the pioneering work of J.Stam who derived a BRDF formulation to modell the effect of far field diffraction for various analytical anisotropic surfaces, relying on the so called scalar wave theory of diffraction for which a wave is assumed to be a complex valued scalar. It's noteworthy that Stam's BRDF formulation does not take into account the polarization of the incident light. Fortunately, light sources like sunlight and light bulbs are unpolarized. The principal beginhind J. Stam's approach is illustrated in figure 1.12.

[11] Image taken from:`http://neutrino.ethz.ch/Vorlesung/FS2013/index.php/vorlesungsskript`, chapter 9, figure 9.14

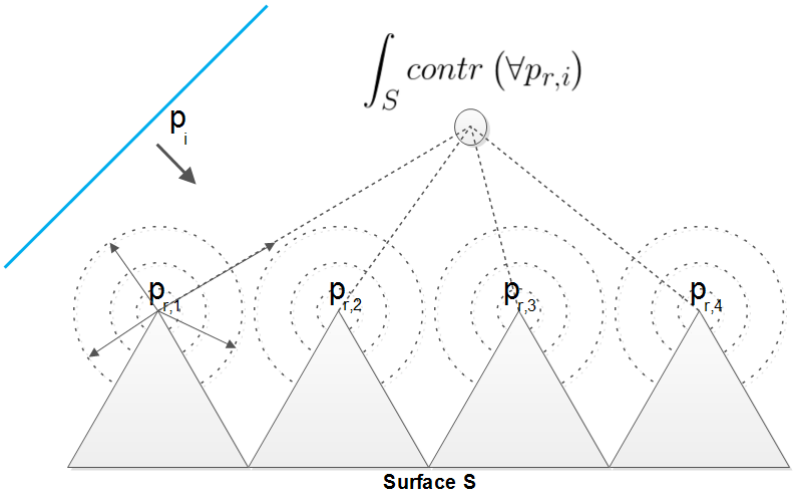

Figure 1.12: Illustration of secondary wavelets reflected off a surface. An integration over all secondary sources resulting from an incident wave according to Huygen's principle will give us an identity for the total contribution at a certain point in space.

An incident wave p_i from a a light source encounters a surface representing a diffraction grating. According to Huygen's Principle, at any point i on the grating at which the incident wave meets the grating a secondary, spherical wavelet $p_{r,i}$ will be emitted. A viewer, indicated by a gray circle in the figure, will perceive the superimposed contribution of all wavelets along the surface S (in the figure indicated by a integration symbol), which will directly follow the laws of wave interference. Therefore the resulting color which an observer sees is the final radiance at that point which reflects from stationary interference of all emitted secondary wavelets and per due to Huygen's principle.

A further assumption in Stam's Paper is, that the emanated waves from the source are stationary, which implies the wave is a superposition of independent monochromatic waves. This further implies that each wave is associated with a definite wavelength λ. Directional light sources such as sunlight fulfill this fact and since we are using these kinds of light sources for our simulations, Stam's model can be used for our modelling purposes.

The main model is the formulate a BRDF as the Fourier Transform applied on the given height field, representing a surface like shown in figure 1.13. The classes of surfaces his model is able to support either exhibit a very regular structure or may be considered as a superposition of bumps forming a periodic like structure. Therefore, the surfaces he is dealing with can either be modelled by probabilistic distributions or have a direct analytical representation. Both cases allow him to derive an analytical solution for his BRDF model.

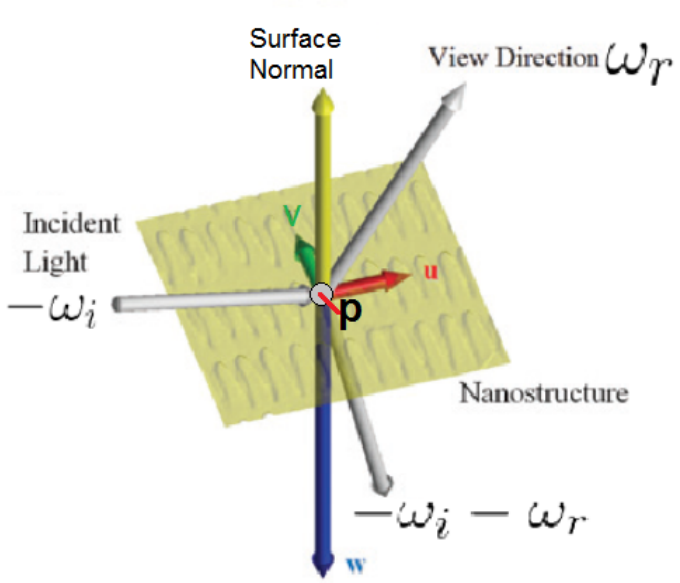

Figure 1.13: Illustration[12] of geometrical setup of Stam's approach where ω_i is a direction, pointing towards the light source, ω_r points towards the camera, n is the surface normal, (u, v, w) are the components of the vector $-\omega_i - \omega_r$.

The direction vector of the secondary wavelet can be computed by taking the difference between the incident and viewing direction like shown in equation 1.5:

$$(u, v, w) = -\omega_i - \omega_r \tag{1.5}$$

These coordinates will later be used in order to compute the total contribution of all secondary sources used in Stam's BRDF in equation 1.8. For simplification, let us introduce an auxiliary function Φ defined in equation 1.6, which models the phase of a wave from the given height field.

$$\Phi(x, y) = \frac{2\pi}{\lambda} wh(x, y) \tag{1.6}$$

Then, any secondary wavelet p which is emitted off from the given surface is equal:

$$p(x, y) = e^{i\Phi(x,y)} \tag{1.7}$$

using the idea presented for figure 1.12 and performing all mathematical steps shown in the appendix **??**, will lead us to the final BRDF representation, modelling the total contribution of all secondary sources reflected off the the provided surface h in the direction ω_r:

$$BRDF_\lambda(\omega_i, \omega_r) = \frac{k^2 F^2 G}{4\pi^2 A w^2} \langle |P(ku, kv)|^2 \rangle \tag{1.8}$$

where F denotes the Fresnel coefficient and G is the so called geometry term[13] which is equal to:

$$G = \frac{(1 + \omega_i \cdot \omega_r)^2}{cos(\theta_i) cos(\theta_r)} \tag{1.9}$$

[12] Modified image which originally has been taken from D.S. Dhillon et. al. poster[DD14].

[13] The geometric terms expresses the correction factor to perform an integration over an area instead over a surface. For further information, please have a look at `http://en.wikipedia.org/wiki/Surface_integral`, and read the definition about *surface element*

One last word about the Fourier transform terms that Stam uses in his derivation: Conventionally, following the definitions of the Fourier Transformation, we are dealing with the inverse Fourier Transformation. However, especially in electrical engineering, it is quite common to define this inverse Fourier transformation by the Fourier Transformation. The reason behind this lies in the fact that we simply could substitute the minus sign as in the following equation 1.10:

$$\begin{aligned}\mathcal{F}_{FT}\{f\}(w) &= \int_{\mathbb{R}^n} f(x)e^{-iwt}dt \\ &= \int_{\mathbb{R}^n} f(x)e^{i\hat{w}t}dt \\ &= \mathcal{F}_{FT}^{-1}\{f\}(w) \end{aligned} \tag{1.10}$$

where $\hat{w}$ is equal $-w$.

The height fields we are dealing with in this work are, however, natural gratings containing a complex shaped nano-structure and hence far from being very regularly aligned. The reason why Stam's approach in its current form is not suitable for our purpose is twofold: First his approach does not capture the complexity of natural gratings accurately well enough when relying on his statistical approaches and secondly it is way too slow in order to be usable for interactive rendering since his BRDF needs an evaluation of a Fourier Transform for every directional changing.

In the following a brief comparison between Stam's[14] and our final approach using two different kinds of gratings, a synthetic, regularly aligned grating and a natural, complex structured grating. These gratings are shown in figure 1.14.

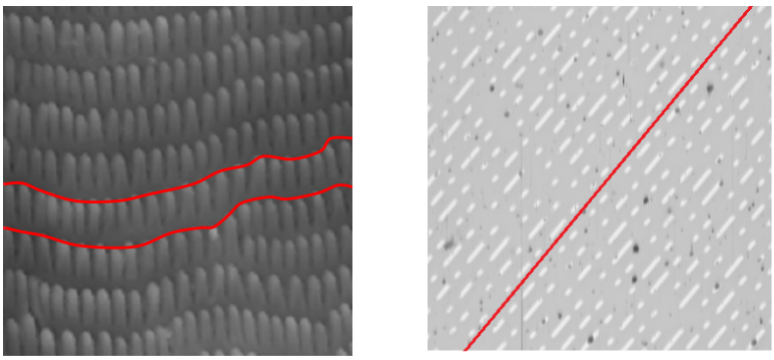

Figure 1.14: Alignment of nano-structures in diffraction gratings. On the left a complex, natural grating of the Elaphe snake species and on the right a synthetic, very regularly aligned grating of a CD.

Figure 1.15 shows an example of a case where Stam's approach performs well. Considering the red-line in the figure we notice that the nano-scaled structures of a compact disc are very regularly aligned along the surface. Tracks of a CD are uniformally spaced and bumps along a track are

[14] A reference implementation of Stam's Diffraction Shader[Sta99] is provided by Nvidia's GPU Gems at `http://http.developer.nvidia.com/GPUGems/gpugems_08.html`

distributed according to a poisson distribution[15]. All angles of the diffraction pattern look the same as in the images produced by our apporach.

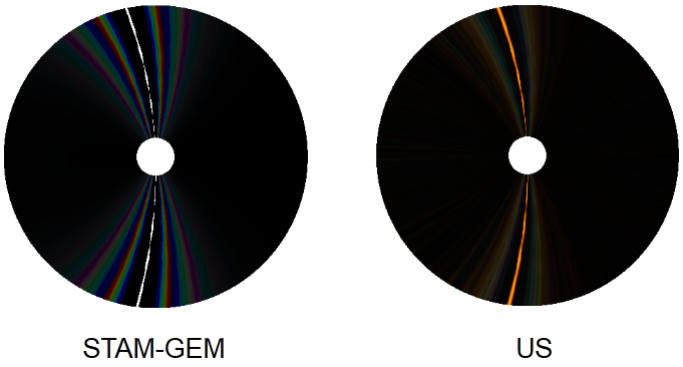

Figure 1.15: Comparison of our approach against a reference implementation of Stam's method provided by Nvida Gem. For synthetic diffraction gratings, which have a very regular structure, Stam's approach is doing well. All angles of the diffraction pattern look the same as in the images produced by our approach.

Figure 1.16 shows an attempt to reproduce real structural colors on the skin of the Xenopeltis snake using our method and comparing it to Stam's approach. Even the results of Stam might look appropriate. However, there are some notable differences such as missing colors close to specular regions, or such as the color distribution which is rather discrete in Stam's approach. Furthermore, Stam's approach has at some places color contribution, where it should not have.

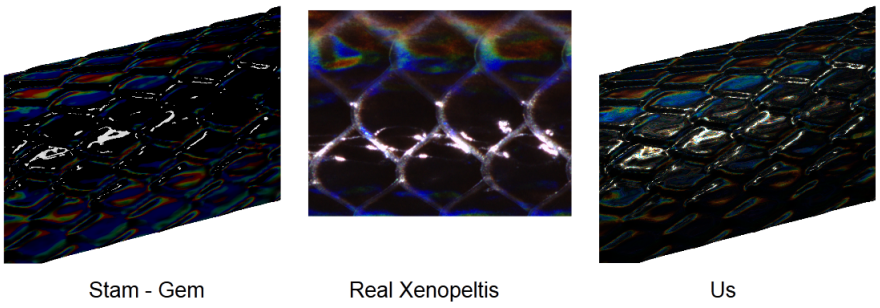

Figure 1.16: Comparison of our approach(on the right) against a reference implementation of Stam's method(on the left) provided by Nvida Gem. We attempt to reproduce a real Xenopeltis skin coloration(center). For natural diffraction gratings, which have a rather complex structure, Stam's approach is qualitatively different from the real image.

In the next chapter we are going to adapt Stam's BRDF model such that it will be able to handle the kind of surfaces we are dealing with and even will have a runtime complexity which permits interactive rendering.

[15]See `http://en.wikipedia.org/wiki/Poisson_distribution`

Chapter 2

Derivations

2.1 Problem Statement and Challenges

The goal of this thesis is to perform a physically accurate and interactive simulation of structural color production as shown in figure 2.2, which we can see whenever light is diffracted from a natural grating. For this purpose we need the following input data (see figure 2.1):

- A mesh representing a snake surface[1] as shown in figure 2.1(a).
- A natural diffraction grating represented as a height field, its maximum height and its pixel width[2].
- A vector field which describes how the given nanostructure patch is oriented on the surface (see figure 2.1(c)).

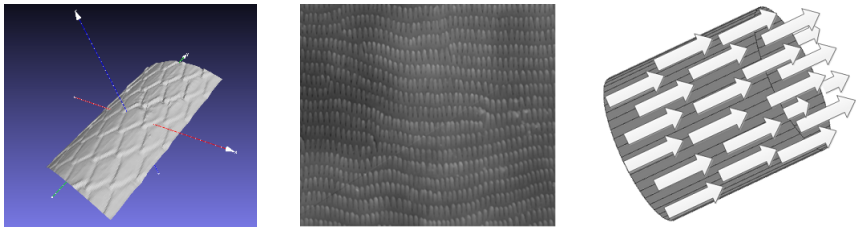

(a) Structure Geometry (b) Nanostructure Surface (c) Patch Orientation

Figure 2.1: Input for our simulation

We want to rely on the integral equation 1.8 derived by J. Stam in his paper [Sta99] about diffraction shaders. This equation formulates a BRDF modelling the effect of diffraction under the assumption that a given grating can either be formulated as an analytical function or its structure is simple enough being modelled relying on statistical methods. These assumptions guarantee that 1.8 has an explicit solution. However, the complexity of a biological nanostructure cannot

[1] In our simulation it is an actual reconstruction of a real snake skin. These measurements are provided by the Laboratory of Artificial and Natural Evolution at Geneva. See their website:`www.lanevol.org`.

[2] Since the nanostructure is stored as a grayscale image, we need a scale telling us what length and height one pixel corresponds to in this provided image.

sufficiently and accurately modelled simply using statistical methods. This is why interactive computation at high resolution becomes a hard task, since we cannot evaluate the given integral equation on the fly. Therefore, we have to adapt Stam's equation such that we are able to perform interactive rendering using explicitly provided height fields at interactive rates.

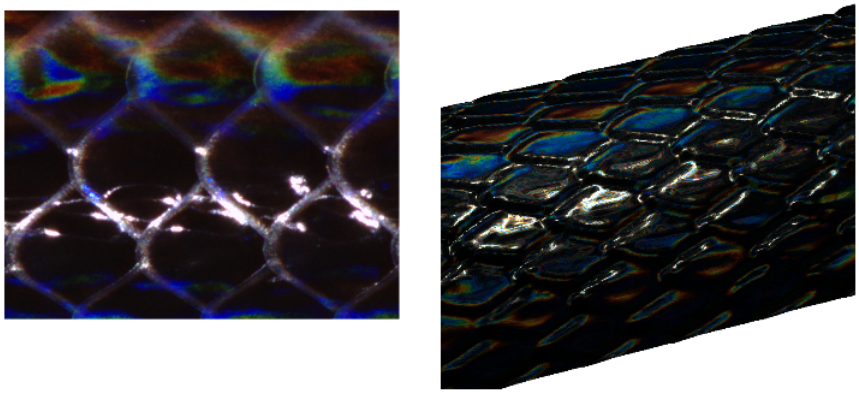

Figure 2.2: Output: Rendered Structural Colors

2.2 Approximate a FT by a DFT

2.2.1 Reproduce FT by DTFT

In the previous section, we have found an identity for the reflected spectral radiance $L_\lambda(\omega_r)$ when using Stam's BRDF for a given input height field. However, the derived expression in equation 2.13 requires to evaluate the Fourier Transform of our height field[3] for every direction. In this section we explain how to approximate the FT by the DTFT and apply it to our previous derivations. Figure 2.3 graphically shows how to obtain the DTFT from the FT for a one dimensional signal[4]

The first step is to uniformly discretize the given signal since computers are working finite, discrete arithmetic. We rely on the Nyquist–Shannon sampling theorem tells us how dense we have to sample a given signal $s(x)$ such that can be reconstructed its sampled version $\hat{s}[n]$[6]. In particular, a sampled version according to the Nyquist–Shannon sampling theorem will have the same Fourier transform as its original signal when it has a limitted bandwidth. The sampling theorem states that if f_{max} denotes the highest frequency of $s(x)$, then, it has to be sampled by a rate of f_s with $2f_{max} \leq f_s$ in order to be reconstructable. By convention $T = \frac{1}{f_s}$ represent the interval length between two samples.

[3] actually it requires the computation of the inverse Fourier Transform of a transformed version of the given height field, the function p(x,y) defined in equation 1.7.

[4] For our case we are dealing with a two dimensional, spatial signal, the given height field. Nevertheless, without any constraints of generality, the explained approach applies to multi dimensional problems.

[5] Images of function plots taken from `http://en.wikipedia.org/wiki/Discrete_Fourier_transform` and are modified.

[6] n denotes the number of samples.

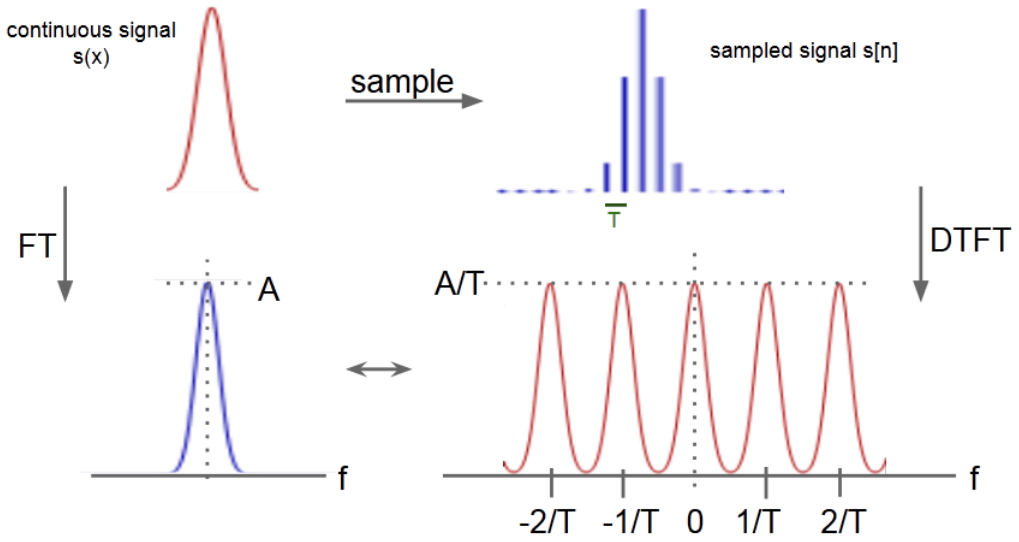

Figure 2.3: Illustration of how to approximate the analytical Fourier Transform (FT) [5] of a given continuous signal by a Discrete Time Fourier Transform (DTFT). The DTFT applied on a band-limited, discretized signal yields a continuous, periodic response in frequency space.

Next, we apply the Fourier transformation operator on the discretized signal $\hat{s}$ which gives us the following expression:

$$\begin{aligned}\mathcal{F}_{FT}\{\hat{s}\}(w) &= \int_{\mathbb{R}} \hat{s}[n]e^{-iwx}dx \\ &= \int_{\mathbb{R}} mask(x)s(x)e^{-iwx}dx \\ &= T\sum_{x=-\infty}^{\infty} \hat{s}[x]e^{-iwx} \\ &= T\mathcal{F}_{DTFT}\{s\}(w) \end{aligned} \tag{2.1}$$

Equation 2.1 tells us that if $\hat{s}$ is sufficiently sampled, then its DTFT corresponds to the FT of $s(x)$. Notice that the resulting DTFT from the sampled signal has a height of $\frac{A}{T}$ where A is the height of the FT of s and thus is a scaled version of the FT.

For a given height field h, let us compute Stam's auxiliary function p defined as in equation 1.7. For the reminder of this thesis we introduce the following definition:

$$P_{dtft} \equiv \mathcal{F}_{DTFT}\{p\} \tag{2.2}$$

Therefore P_{dtft} denotes the DTFT of a transformed version of our height field h [7].

[7] By transformed height field we mean $p(x,y) = e^{i\frac{2\pi}{\lambda}wh(x,y)}$ which we get, when we plug h into equation 1.6 and this expression again plug into equation 1.7.

2.2.2 Spatial Coherence and Windowing

Before we can derive a final expression in order to approximate a FT by a DFT, we first have to revisit the concept of coherence introduced in section 1.2.3 of chapter 2. Previously we have seen that wave-theory tells us what is the total contribution of all secondary sources which allows us to say what is the reflected spectral radiance at a certain point in space. This is related to stationary interference which itself depends on the coherence property of the emitted secondary wave sources. The ability for two points in space, t_1 and t_2, to interfere in the extend of a wave when being averages over time is the so called spatial coherence. The spatial distance between such two points over which there is significant interference is limited by the quantity coherence area. For filtered sunlight on earth this is equal to $65\mu m$ [8].

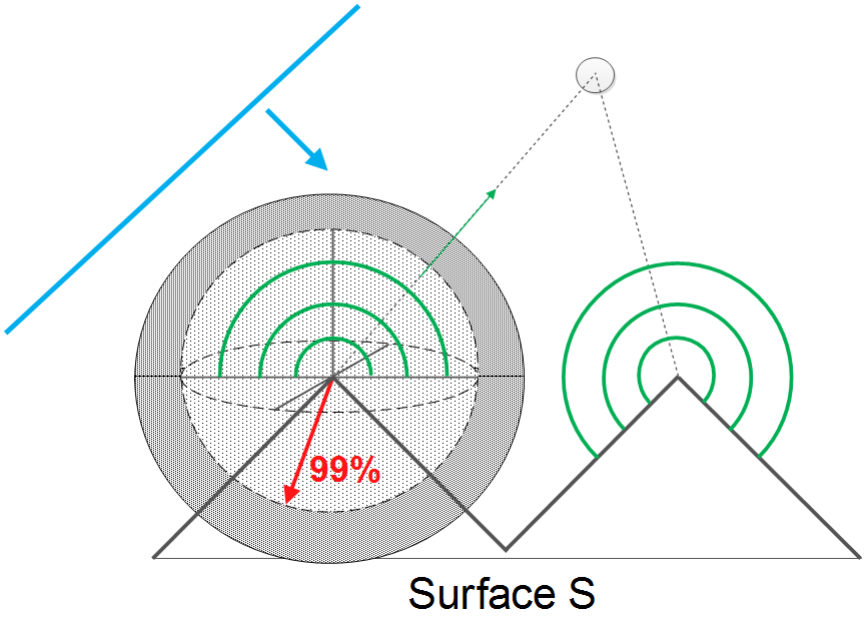

Figure 2.4: A plane wave encounters a surface. According to Huygens principle, secondary wavelets are emitted of from this surface. The resulting wave at a certain point in space (here indicated by a gray circle) depends on the interference among all waves encountering at this position. The amount of significant interference is directly affected by the spatial coherence property of all the wavelets.

Figure 2.4 illustrates the concept of spatial coherence. A wavefront (blue line) encounters a surface. Due to Huygen's principle, secondary wavelets are emitted off from the surface. The reflected radiance at a certain point in space, e.g. at a viewer's eye position (denoted by the gray circle), is a result of interference among all wavelets at that point. This interference is directly affected by the spatial coherence property of all the emitted wavelets.

In physics spatial coherence is predicted by the cross correlation between t_1 and t_2 and usually modelled by a Gaussian Random Process. For any such Gaussian Process we can use a spatial gaussian window $g(x)$ which is equal:

[8] A proof for this number can be looked up in the book Optical Coherence and Quantum Optics[LM95] on page 153 and 154.

$$g(x) = \frac{1}{\sqrt{2\pi} \cdot \sigma} \cdot e^{-\frac{x^2}{2\sigma^2}} \tag{2.3}$$

We have chosen standard deviation σ_s of the window such that it fulfills the equation $4\sigma_s = 65\mu m$. This is equivalent to saying that we want to predict about 99.99%[9] of the resulting spatial coherence interference effects in our model by a cross correlation function.

By applying the Fourier transformation to the spatial window we get the corresponding window in frequency space as:

$$G(f) = e^{-\frac{f^2}{2\sigma_f^2}} \tag{2.4}$$

Notice that this frequency space window has a standard deviation σ_f equal to $\frac{1}{2\pi\sigma_s}$. Those two windows, the spatial- and the frequency space window, will be used in the next section in order to approximate the DTFT by the DFT by a windowing approach.

2.2.3 Reproduce DTFT by DFT

In this section we explain how and under what assumptions the DTFT of a discretized signal[10] can be approximated by a DFT. The whole idea how to reproduce the DTFT by DFT is schematically illustrated in figure 2.5.

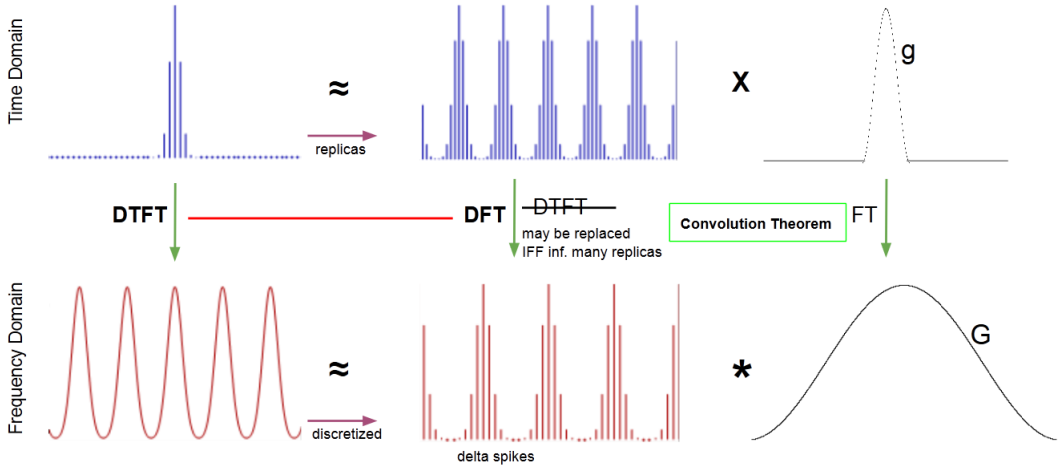

Figure 2.5: Illustration of how to approximate the DTFT [11] by the DFT relying on the Convolution Theorem, using a gaussian window function.

Lets say, we are given a spatial, band-limited and discretized one dimensional signal $\hat{s}$. Our goal is to approximate this spatial signal in a way such that when taking the DFT of this approximated signal, it will yield the same response as taking the DTFT of the original sampled $\hat{s}$. For

[9] Standard deviation values from confidence intervals table of normal distribution provided by Wolfram MatheWorld `http://mathworld.wolfram.com/StandardDeviation.html`.

[10] E.g. a sampled signal like already presented in figure 2.3

[11] Images of function plots taken from `http://en.wikipedia.org/wiki/Discrete_Fourier_transform` and are modified. Note that the scales in the graphic are not appropriate.

this purpose we will use the previously introduced concept of gaussian windows and the so called Convolution Theorem which is a fundamental property of all Fourier transformations.

The Convolution Theorem states that the Fourier transformation of a product of two functions, f and g, is equal to convolving the Fourier Transformations of each individual function. Mathematically, this statement corresponds to equation 2.5:

$$\mathcal{F}\{f \cdot g\} = \mathcal{F}\{f\} * \mathcal{F}\{g\} \tag{2.5}$$

The principal issue is how to approximate our given signal $\hat{s}$. Therefore, let us consider another signal $\hat{s_N}$ which is the N times replicated version of $\hat{s}$ (blue signal at center top in figure).

Remember that, in general, the wave magnitude at a certain point in space is the result of interference among all wavelength meeting at that position. In our scenario, the source of those signals are emitted secondary wavelets. The interference strength between wavelets is related to their spatial coherence. Windowing the signal by a gaussian window g is akin to modelling the effects of spatial coherence interference on the surface. From the previous section 2.2.2 we know that we can use gaussian window like in equation 2.3 in order to approximate such spatial signals interference effects.

Using this insight, we can approximate $\hat{s}$ by taking the product of $\hat{s_N}$ with a gaussian window g. This fact is illustrated in the first row of figure 2.3. So, what will the DTFT of this approximation yield? We already know that the DTFT of $\hat{s}$ is a continuous, periodic signal, since $\hat{s}$ is band-limited. Thus, taking the DTFT of this found approximation should give us approximatively the same continuous, periodic signal.

This is where the convolution theorem comes into play: Applying the DTFT to the product of $\hat{s_N}$ and g is the same as convolving the DTFT of $\hat{s_N}$ by DTFT of g. From equation 2.4 we already know that the DTFT of g is just another gaussian, denoted by G. On the other hand the DTFT of $\hat{s_N}$ yields a continuous, periodic signal. The higher the value of N, the sharper the signal gets (denoted by delta spiked) and the closer it converges toward to the DFT. This is why the DFT is the limit of a DTFT applied on periodic and discrete signals. Therefore, for a large number of N we can replace the DTFT by the DFT operator when applied on $\hat{s_N}$.

Lastly, we see that the DTFT of $\hat{s}$ is approximately the same like convolving a gaussian window by the DFT of $\hat{s_N}$. This also makes sense, since convolving a discrete, periodic signal (DFT of $\hat{s_N}$) by a continuous window function G yields a continuous, periodic function.

In general, for every non-windowed signal, we cannot compute its DTFT **??** numerically due to finite computer arithmetic and hence working with the DFT is our only option. Furthermore, there are numerically fast algorithms in order to compute the DFT values of a function, the Fast Fourier Transformation (FFT). The DFT **??** of a discrete height field is equal to the DTFT of an infinitely periodic function consisting of replicas of the same height field. Now, let a spatial gaussian window g having a standard deviation for which $4\sigma_s$ is equal $65\mu m$. Then, from before, it follows:

$$\mathcal{F}_{dtft}\{\mathbf{s}\} \equiv \mathcal{F}_{dft}\{\mathbf{s}\} * G(\sigma_f) \tag{2.6}$$

Therefore we can deduce the following expression:

$$\begin{aligned}
\mathcal{F}_{dtft}\{\mathbf{t}\}(u,v) &= \int_{-\infty}^{\infty}\int_{-\infty}^{\infty} F_{dft}\{\mathbf{t}\}(w_u,w_v)\phi(u-w_u,v-w_v)dw_u dw_v \\
&= \int_{-\infty}^{\infty}\int_{-\infty}^{\infty} \sum_i\sum_j F_{dft}\{\mathbf{t}\}(w_u,w_v) \\
&\quad \delta(w_u-w_i,w_v-w_j)\phi(u-w_u,v-w_v)dw_u dw_v \\
&= \sum_i\sum_j \int_{-\infty}^{\infty}\int_{-\infty}^{\infty} F_{dft}\{\mathbf{t}\}(w_u,w_v) \\
&\quad \delta(w_u-w_i,w_v-w_j)\phi(u-w_u,v-w_v)dw_u dw_v \\
&= \sum_i\sum_j F_{dft}\{\mathbf{t}\}(w_u,w_v)\phi(u-w_u,v-w_v) \qquad (2.7)
\end{aligned}$$

where

$$\phi(x,y) = \pi e^{-\frac{x^2+y^2}{2\sigma_f^2}} \qquad (2.8)$$

2.3 Adaption of Stam's BRDF for Discrete Height Fields

2.3.1 Rendering Equation

As already discussed in the theoretical background chapter, colors are associated to radiance. Since we are starting with Stam's BRDF[12] formulation but want to perform a simulation rendering structural colors, we have to reformulate this BRDF equation such that we will end up with an identity of the reflected spectral radiance. This is where the rendering equation comes into play. Let us assume we are given an incoming light source directional at a solid angle ω_i and θ_i is its angle of incidence and that ω_r is the solid angle for the viewing direction. Further let λ denote the wavelength[13] and Ω is the hemisphere of integration for the incoming light. Then, we are able to formulate a $BRDF_\lambda$ by using its definition 1.3:

$$\begin{aligned}
& f_r(\omega_i,\omega_r) && = \frac{dL_r(\omega_r)}{L_i(\omega_i)cos(\theta_i)d\omega_i} \\
\Rightarrow\ & f_r(\omega_i,\omega_r)L_i(\omega_i)cos(\theta_i)d\omega_i && = dL_r(\omega_r) \\
\Rightarrow\ & \int_\Omega f_r(\omega_i,\omega_r)L_i(\omega_i)cos(\theta_i)d\omega_i && = \int_\Omega dL_r(\omega_r) \\
L_r(\omega_r) & && \Longrightarrow \int_\Omega f_r(\omega_i,\omega_r)L_i(\omega_i)cos(\theta_i)d\omega_i \qquad (2.9)
\end{aligned}$$

The last equation is the so called rendering equation . We assume that our incident light is a directional, unpolarized light source like sunlight and therefore its radiance is given as

$$L_\lambda(\omega) = I(\lambda)\delta(\omega-\omega_i) \qquad (2.10)$$

[12]Remember that a BRDF is the portion of a incident light source reflected off a given surface towards a specified viewing direction.

[13]Notice that, to keep our terms simple, we have dropped all λ subscripts for spectral radiance quantities.

where $I(\lambda)$ is the intensity of the relative spectral power for the wavelength λ. By plugging the identity in equation 2.10 into our current rendering equation 2.9, we will get:

$$\begin{aligned} L_\lambda(w_r) &= \int_\Omega BRDF_\lambda(\omega_i, \omega_r) L_\lambda(\omega_i) cos(\theta_i) d\omega_i \\ &= BRDF_\lambda(\omega_i, \omega_r) I(\lambda) cos(\theta_i) \end{aligned} \tag{2.11}$$

where $L_\lambda(\omega_i)$ is the incident radiance and $L_\lambda(\omega_r)$ is the radiance reflected by the given surface. Note that the integral in equation 2.11 vanishes since $\delta(\omega - \omega_i)$ is only equal one if and only if $\omega = \omega_i$.

2.3.2 Reflected Radiance of Stam's BRDF

We are going to use Stam's main derivation (1.8) for the $BRDF(\omega_i, \omega_r)$ in 2.11 by applying the fact that the wavenumber is equal $k = \frac{2\pi}{\lambda}$:

$$\begin{aligned} BRDF(\omega_i, \omega_r) &= \frac{k^2 F^2 G}{4\pi^2 A w^2} \langle |P(ku, kv)|^2 \rangle \\ &= \frac{4\pi^2 F^2 G}{4\pi^2 A \lambda^2 w^2} \langle |P(ku, kv)|^2 \rangle \\ &= \frac{F^2 G}{A \lambda^2 w^2} \langle \left| P(\frac{2\pi u}{\lambda}, \frac{2\pi v}{\lambda}) \right|^2 \rangle \end{aligned} \tag{2.12}$$

Going back to equation 2.11 and plugging equation 2.12 into it, using the definition of equation 1.9 and the equation **??** for ω we will get the following:

$$\begin{aligned} L_\lambda(\omega_r) &= \frac{F^2 (1 + \omega_i \cdot \omega_r)^2}{A \lambda^2 cos(\theta_i) cos(\theta_r) \omega^2} \left\langle \left| P\left(\frac{2\pi u}{\lambda}, \frac{2\pi v}{\lambda}\right) \right|^2 \right\rangle cos(\theta_i) I(\lambda) \\ &= I(\lambda) \frac{F^2 (1 + \omega_i \cdot \omega_r)^2}{\lambda^2 A \omega^2 cos(\theta_r)} \left\langle \left| P\left(\frac{2\pi u}{\lambda}, \frac{2\pi v}{\lambda}\right) \right|^2 \right\rangle \end{aligned} \tag{2.13}$$

Note that the Fresnel term F is actually a function of (w_i, w_r), but in order to keep the equations simple, we omitted its arguments.

So far we just plugged Stam's BRDF identity into the rendering equation and hence have not significantly deviated from his formulation. Keep in mind that P denotes the Fourier transform of the provided height field which depends on the viewing and incidence light direction. Thus this Fourier Transform has to be recomputed for every direction which will slow down the whole computation quite a lot[14]. One particular strategy to solve this issue is to approximate P by the Discrete Fourier Transform (DFT)[15] and separate its computation such that terms for many directions can be precomputed and then later retrieved by look ups. The approximation of P happens in two steps: First we approximate the Fourier Transform by the Discrete Time Fourier Transform (DTFT) and then, afterwards, we approximate the DTFT by the DFT. For further about basics

[14] Even a fast variant of computation the Fourier Transform has a runtime complexity of O(N log N) where N is the number of sample.

[15] See appendix **??** for further information about different kinds of Fourier transformations.

of signal processing and Fourier Transformations please consult the appendix **??**.

Using the insight gained by equation 2.1 allows us to further simplify equation 2.13:

$$\begin{aligned} L_\lambda(\omega_r) &= I(\lambda)\frac{F^2(1+\omega_i\cdot\omega_r)^2}{\lambda^2 A w^2 cos(\theta_r)}\left\langle\left|P\left(\frac{2\pi u}{\lambda},\frac{2\pi v}{\lambda}\right)\right|^2\right\rangle \\ &= I(\lambda)\frac{F^2(1+\omega_i\cdot\omega_r)^2}{\lambda^2 A w^2 cos(\theta_r)}\left\langle\left|T^2 P_{dtft}\left(\frac{2\pi u}{\lambda},\frac{2\pi v}{\lambda}\right)\right|^2\right\rangle \end{aligned} \tag{2.14}$$

Where P_{dtft} is a substitute for $\mathcal{F}_{DTFT}\{s\}(w)$. Furthermore T the sampling distance for the discretization of $p(x,y)$ assuming equal and uniform sampling in both dimensions x and y.

2.3.3 Relative Reflectance

In this section we are going to explain how to scale our BRDF formulation such that all of its possible output values are mapped into the range $[0,1]$. Such a relative reflectance formulation will ease our life for later rendering purposes since usually color values are within the range $[0,1]$, too. Furthermore, this will allow us to properly blend the resulting illumination caused by diffraction with a texture map.

Let us examine what $L_\lambda(\omega_r)$ will be for a purely specular surface, for which $\omega_r = \omega_0 = \omega_i$ such that $\omega_0 = (0,0,1)$. For this specular reflection case, the corresponding radiance will be denoted as $L_\lambda^{spec}(\omega_0)$. We define the relative reflected radiance for our problem 2.13 by simply taking the fraction between $L_\lambda(\omega_r)$ and $L_\lambda^{spec}(\omega_0)$ which is denoted by:

$$\rho_\lambda(\omega_i,\omega_r) = \frac{L_\lambda(\omega_r)}{L_\lambda^{spec}(\omega_0)} \tag{2.15}$$

Notice that the third component w from the vector in equation 1.5 is squared equal to $(cos(\theta_i) + cos(\theta_r))^2$[16]. But first, let us derive the following expression:

$$\begin{aligned} L_\lambda^{spec}(\omega_0) &= I(\lambda)\frac{F(\omega_0,\omega_0)^2(1+\begin{pmatrix}0\\0\\1\end{pmatrix}\cdot\begin{pmatrix}0\\0\\1\end{pmatrix})^2}{\lambda^2 A(cos(0)+cos(0))^2 cos(0)}\langle\left|T_0^2 P_{dtft}(0,0)\right|^2\rangle \\ &= I(\lambda)\frac{F(\omega_0,\omega_0)^2(1+1)^2}{\lambda^2 A(1+1)^2 1}\left|T_0^2 N_{sample}\right|^2 \\ &= I(\lambda)\frac{F(\omega_0,\omega_0)^2}{\lambda^2 A}\left|T_0^2 N_{sample}\right|^2 \end{aligned} \tag{2.16}$$

Where $N_{samples}$ is the number of samples of the DTFT **??**. Thus, we can plug our last derived expression 2.16 into the definition for the relative reflectance radiance 2.15 in the direction w_r and we get:

[16] Consult section **??** in the appendix

$$\begin{aligned}\rho_\lambda(\omega_i,\omega_r) &= \frac{L_\lambda(\omega_r)}{L_\lambda^{spec}(\omega_0)} \\ &= \frac{I(\lambda)\frac{F(\omega_i,\omega_r)^2(1+\omega_i\cdot\omega_r)^2}{\lambda^2 A(cos(\theta_i)+cos(\theta_r))^2 cos(\theta_r)}\langle\left|T_0^2 P_{dtft}(\frac{2\pi u}{\lambda},\frac{2\pi v}{\lambda})\right|^2\rangle}{I(\lambda)\frac{F(\omega_0,\omega_0)^2}{\lambda^2 A}\left|T_0^2 N_{sample}\right|^2} \\ &= \frac{F^2(\omega_i,\omega_r)(1+\omega_i\cdot\omega_r)^2}{F^2(\omega_0,\omega_0)(cos(\theta_i)+cos(\theta_r))^2 cos(\theta_r)}\langle\left|\frac{P_{dtft}(\frac{2\pi u}{\lambda},\frac{2\pi v}{\lambda})}{N_{samples}}\right|^2\rangle \end{aligned} \tag{2.17}$$

For simplification and better readability, let us define the following gain-factor:

$$C(\omega_i,\omega_r) = \frac{F^2(\omega_i,\omega_r)(1+\omega_i\cdot\omega_r)^2}{F^2(\omega_0,\omega_0)(cos(\theta_i)+cos(\theta_r))^2 cos(\theta_r) N_{samples}^2} \tag{2.18}$$

Using equation 2.18, we get the following expression for the relative reflectance radiance from equation 2.17:

$$\rho_\lambda(\omega_i,\omega_r) = C(\omega_i,\omega_r)\langle\left|P_{dtft}(\frac{2\pi u}{\lambda},\frac{2\pi v}{\lambda})\right|^2\rangle \tag{2.19}$$

Using the previous definition for the relative reflectance radiance equation 2.15:

$$\rho_\lambda(\omega_i,\omega_r) = \frac{L_\lambda(\omega_r)}{L_\lambda^{spec}(\omega_0)}$$

Which we can rearrange to the expression:

$$L_\lambda(\omega_r) = \rho_\lambda(\omega_i,\omega_r) L_\lambda^{spec}(\omega_0) \tag{2.20}$$

Let us choose $L_\lambda^{spec}(w_0) = S(\lambda)$ such that is has the same profile as the relative spectral power distribution of CIE Standard Illuminant $D65$ discussed in **??**. Furthermore, when integrating over λ for a specular surface, we should get CIE_{XYZ} values corresponding to the white point for $D65$. The corresponding tristimulus values using CIE colormatching functions 1.4 for the CIE_{XYZ} values look like:

$$\begin{aligned} X &= \int_\lambda L_\lambda(\omega_r)\overline{x}(\lambda)d\lambda \\ Y &= \int_\lambda L_\lambda(\omega_r)\overline{y}(\lambda)d\lambda \\ Z &= \int_\lambda L_\lambda(\omega_r)\overline{z}(\lambda)d\lambda \end{aligned} \tag{2.21}$$

where $\overline{x}$, $\overline{y}$, $\overline{z}$ are the color matching functions. Combining our last finding from equation 2.20 for $L_\lambda(\omega_r)$ with the definition of the tristimulus values from equation 2.21, allows us to derive a formula for computing the colors values using Stam's BRDF formula relying on the rendering equation 2.9. Without any loss of generality it suffices to derive an explicit expression for just one tristimulus term, for example Y, the luminance:

$$
\begin{aligned}
Y &= \int_\lambda L_\lambda(\omega_r)\overline{y}(\lambda)d\lambda \\
&= \int_\lambda \rho_\lambda(\omega_i,\omega_r)L_\lambda^{spec}(\omega_0)\overline{y}(\lambda)d\lambda \\
&= \int_\lambda \rho_\lambda(\omega_i,\omega_r)S(\lambda)\overline{y}(\lambda)d\lambda \\
&= \int_\lambda C(\omega_i,\omega_r)\langle\left|P_{dtft}(\frac{2\pi u}{\lambda},\frac{2\pi v}{\lambda})\right|^2\rangle S(\lambda)\overline{y}(\lambda)d\lambda \\
&= C(\omega_i,\omega_r)\int_\lambda \langle\left|P_{dtft}(\frac{2\pi u}{\lambda},\frac{2\pi v}{\lambda})\right|^2\rangle S(\lambda)\overline{y}(\lambda)d\lambda \\
&= C(\omega_i,\omega_r)\int_\lambda \langle\left|P_{dtft}(\frac{2\pi u}{\lambda},\frac{2\pi v}{\lambda})\right|^2\rangle S_y(\lambda)d\lambda
\end{aligned} \tag{2.22}
$$

Where we used the definition $S_y(\lambda)\overline{y}(\lambda)$ in the last step.

2.4 Optimization using Taylor Series

Our final goal is to render structural colors resulting by the effect of wave diffraction. So far, we have derived an expression which can be used for rendering. Nevertheless, our current equation 2.22 used for computing structural colors, cannot directly be used for interactive rendering, since P_{dtft} had do be recomputed for every change in any direction[17].

In this section, we will address this issue and deliver an approximation for P_{dtft} defined in equation 2.2. This approximation will allow us to separate P_{dtft} in a certain way such that some computional expensive terms can be precomputed. The main idea is to formulate P_{dtft} as a series expansion relying on the definition of Taylor Series, like defined in equation **??**. Further, we will provide an error bound for our approximation approach for a given number of terms. Last, we will plug our finding extend our current BRDF formula from equation 2.22 by the findings derived within this section.

Let us consider $p(x,y) = e^{ikwh(x,y)}$ form Stam's Paper 1.3 where $h(x,y)$ is a given height field and $k = \frac{2\pi}{\lambda}$ denotes the wavenumber of wavelength λ. For any complex number t the power series expansion of the exponential function is equal to:

$$
e^t = 1 + t + \frac{t^2}{2!} + \frac{t^3}{3!} + ... = \sum_{n=0}^{\infty}\frac{t^n}{n!} \tag{2.23}
$$

Now, when we use the exponent[18] of $p(x,y)$ as an input argument for equation 2.23 we get:

[17] According to changes in viewing- or incident light direction.

[18] This exponent is a complex valued function, equal to ikwh(x,y).

$$\begin{aligned} e^t &= e^{ikwh} \\ &= 1 + (ikwh) + \frac{1}{2!}(ikwh)^2 + \frac{1}{3!}(ikwh)^3 + ... \\ &= \sum_{n=0}^{\infty} \frac{(ikwh)^n}{n!}. \end{aligned} \tag{2.24}$$

where i is the imaginary unit for complex numbers. For simplification, in the reminder of this section we omitted the arguments of h. Equation 2.24 gives us an expression for an exponential series expansion for an for the exponent of $p(x,y)$. Please note that above's taylor series is convergent for any complex valued number. Therefore the equation 2.24 is equal to

$$p(x,y) = \sum_{n=0}^{\infty} \frac{(ikwh(x,y))^n}{n!} \tag{2.25}$$

and thus gives us a series representation of $p(x,y)$. Next, calculating the Fourier Transformation $\mathcal{F}$ of equation 2.25 gives us the identity:

$$\begin{aligned} \mathcal{F}\{p\} &\equiv \mathcal{F}\left\{ \sum_{n=0}^{\infty} \frac{(ikwh)^n}{n!}. \right\} \\ &\equiv \sum_{n=0}^{\infty} \mathcal{F}\left\{ \frac{(ikwh)^n}{n!} \right\} \\ &\equiv \sum_{n=0}^{\infty} \frac{(ikw)^n}{n!} \mathcal{F}\{h^n\} \end{aligned} \tag{2.26}$$

Where we have exploited the fact that the Fourier Transformation is a linear operator. Therefore, in equation 2.26, we have shown that the Fourier Transformation of a series is equal to the sum of the Fourier Transformation, applied on each individual series term. Reusing the identifier P[19] in order to determine the Fourier Transformation of Stams definition p from equation 1.7, equation 2.26 then correspond to:

$$P(\alpha,\beta) = \sum_{n=0}^{\infty} \frac{(ikw)^n}{n!} \mathcal{F}\{h^n\}(\alpha,\beta) \tag{2.27}$$

Up to now we have found a infinity series representation for P_{dtft}. Next we are going to look for an upper bound $N \in \mathbb{N}$ such that

$$\tilde{P}_N(\alpha,\beta) := \sum_{n=0}^{N} \frac{(ikwh)^n}{n!} \mathcal{F}\{h^n\}(\alpha,\beta) \approx P(\alpha,\beta) \tag{2.28}$$

$\tilde{P}_N$ is a good approximation of P, i.e. their absolute difference is small[20]. But first, the following two facts would have to be proven[21]:

1. Show that there exist such an $N \in \mathbb{N}$ s.t. the approximation of equation 2.28 holds true.

[19] This identifier P may be subscripted by *dtft* which will denote the DTFT variant of P.
[20] Mathematically speaking, this statement correspond to $||\tilde{P}_N - P|| \leq \epsilon$, where $\epsilon > 0$ is a small number.
[21] Please have a look in section **??** in the appendix

2. Find a value for N s.t. this approximation is below a certain error bound, e.g. close to machine precision ϵ.

Assuming these facts are valid and proven (see appendix **??**) implies that there actually exists such an N. Thus, we can make use of the taylor series approximation from equation 2.28 and use it for approximating P_{dtft}. This idea allows us to adapt equation 2.22, which is used for computing the structural colors of our BRDF model, in numerically fast way. E.g. the equation for the luminance is then be equal:

$$\begin{aligned} Y &= C(w_i, w_r) \int_\lambda \langle \left| P_{dtft}(\frac{2\pi u}{\lambda}, \frac{2\pi v}{\lambda}) \right|^2 \rangle S_y(\lambda) d\lambda \\ &= C(w_i, w_r) \int_\lambda \left| \sum_{n=0}^{N} \frac{(wk)^n}{n!} \mathcal{F}\{i^n h^n\}(\frac{2\pi u}{\lambda}, \frac{2\pi v}{\lambda}) \right|^2 S_y(\lambda) d\lambda \end{aligned} \tag{2.29}$$

Notice that equation 2.29 is constrained by N and hence is an approximation of equation 2.22. Furthermore, it is possible to seperate out all the Fourier Terms in the summation and precompute them. This is why the approach in equation 2.29 is fast in order to compute structural color values according to our BRDF model.

2.5 Spectral Rendering

In this section we describe how our final model for rendering structural colors due to diffraction will look like. For this purpose we use all our previous findings and plug them together to one big equation. For a given height field h representing the surface of a grating, we want to compute the resulting color due to light diffracted on that grating. For rendering we rely on the CIE_{XYZ} colorspace. For given direction vectors w_i and w_r as shown in figure 1.13 the DFT of the height field is equal to:

$$DFT_n\{h\}(u, v) = F_{dft}\{i^n h^n\}(\frac{2\pi u}{\lambda}, \frac{2\pi v}{\lambda}) \tag{2.30}$$

From section 2.2.3 we know that we can reproduce a FT by applying a Gaussin window on the DFT from equation 2.30. This Windowing approach will then look like:

$$W_n(u, v) = \sum_{(r,s) \in \mathcal{N}_1(u,v)} |DFT_n\{h\}(u - w_r, v - w_s)|^2 \phi(u - w_r, v - w_s) \tag{2.31}$$

where $\phi(x, y) = \pi e^{-\frac{x^2+y^2}{2\sigma_f^2}}$ is the Gaussian window from equation 2.2.3 and $\mathcal{N}_1(u, v)$ denotes the one-neighborhood around (u, v).

In section 2.4 we derived equation 2.29 which tells us how to compute the CIE_{XYZ} color value of a particular color channel using our relative reflectance brdf model from section 2.3.3. Plugging all these findings together and using our windowing approach, listed in equation 2.31, Then $\forall(u, v, w)$ like (defined in equation 1.5), our final expression for computing structural colors due to diffraction, using all our previous derivations, will be equal:

$$\begin{pmatrix} X \\ Y \\ Z \end{pmatrix} = C(\omega_i, \omega_r) \int_\Lambda \sum_{n=0}^{N} \frac{(2\pi w)^n}{\lambda^n n!} W_n(u, v) \begin{pmatrix} S_x(\lambda) \\ S_y(\lambda) \\ S_z(\lambda) \end{pmatrix} d\lambda \tag{2.32}$$

Where $C(\omega_i, \omega_r)$ is the defined in equation 2.18. Note that equation 2.32 integrates over a given wavelength spectrum, denoted by Λ. Usually, this Λ is equal to $[\lambda_{min}, \lambda_{max}]$ where $\lambda_{min} = 380nm$ and $\lambda_{max} = 780nm$.

2.6 Alternative Approach

2.6.1 PQ factors

In this section we are presenting an alternative approach to the previous Gaussian window approach described in section 2.2.3 in order to solve the issue working with $DTFT$ instead the DFT. We assume, that a given surface S is covered by a number of replicas of a provided representative surface patch f. In a simplified, one dimensional scenario, mathematically speaking, f is assumed to be a repetitive function, i.e. $\forall x \in \mathbb{R} : S(x) = S(x + nT)$, where T is its period and $n \in \mathbb{N}_0$. Thus, the surfaces can be written formally as:

$$S(x) = \sum_{n=0}^{N} f(x + nT) \tag{2.33}$$

What we are looking for is an identity for the Fourier Transform[22] of our surface S, required in order to simplify the (X, Y, Z) colors from 2.29:

$$\begin{aligned} \mathcal{F}\{S\}(w) &= \int f(x) e^{iwx} dx \\ &= \int_{-\infty}^{\infty} \sum_{n=0}^{N} f(x + nT) e^{iwx} dx \\ &= \sum_{n=0}^{N} \int_{-\infty}^{\infty} f(x + nT) e^{iwx} dx \end{aligned} \tag{2.34}$$

Next, apply the following substitution $x + nT = y$ which will lead us to:

$$\begin{aligned} x &= y - nT \\ dx &= dy \end{aligned} \tag{2.35}$$

Plugging this substitution back into equation 2.34 we will get:

[22] Remember that we are using the definition of Fourier Transform used in electrical engineering where $\mathcal{F}$ actually corresponds to the inverse Fourier Transform.

$$\begin{aligned}\mathcal{F}\{S\}(w) &= \sum_{n=0}^{N} \int_{-\infty}^{\infty} f(x+nT)e^{iwx}dx \\ &= \sum_{n=0}^{N} \int_{-\infty}^{\infty} f(y)e^{iw(y-nT)}dy \\ &= \sum_{n=0}^{N} e^{-iwnT} \int_{-\infty}^{\infty} f(y)e^{iwy}dy \\ &= \sum_{n=0}^{N} e^{-iwnT}\mathcal{F}\{f\}(w) \\ &= \mathcal{F}\{f\}(w) \sum_{n=0}^{N} e^{-iwnT} \end{aligned} \tag{2.36}$$

We used the fact that the exponential term e^{-iwnT} is a constant factor when integrating along dy and the identity for the Fourier Transform of the function f. Next, let us examine the series $\sum_{n=0}^{N} e^{-iwnT}$ closer:

$$\begin{aligned}\sum_{n=0}^{N} e^{-uwnT} &= \sum_{n=0}^{N} (e^{-iwT})^n \\ &= \frac{1-e^{iwT(N+1)}}{1-e^{-iwT}} \end{aligned} \tag{2.37}$$

We recognize the geometric series identity for the left-hand-side of equation 2.37. Mainly relying on trigonometric identities, equation 2.36 can further simplified to:

$$\mathcal{F}\{S\}(w) = (p+iq)\mathcal{F}\{f\}(w) \tag{2.38}$$

where p and q are defined like:

$$\begin{aligned} p &= \frac{1}{2} + \frac{1}{2}\left(\frac{cos(wTN) - cos(wT(N+1))}{1-cos(wT)}\right) \\ q &= \frac{sin(wT(N+1)) - sin(wTN) - sin(wT)}{2(1-cos(wT))} \end{aligned} \tag{2.39}$$

Please notice, all derivation steps can be found in the appendix in section **??**.

Now lets consider our actual problem description. Given a patch of a nano-scaled surface snake shed represented as a two dimensional height field $h(x,y)$. We once again assume that this provided patch is representing the whole surface S of our geometry by some number of replicas of itself. Therefore, $S(x,y) = \sum_{n=0}^{N} h(x+nT_1, y+mT_2)$, assuming the given height field has the dimensions T_1 by T_2. In order to derive an identity for the two dimensional Fourier transformation of S we can similarly proceed like we did to derive equation 2.38.

$$\mathcal{F}\{S\}(w_1,w_2) = (p+iq)\mathcal{F}_{DTFT}\{h\}(w_1,w_2) \tag{2.40}$$

Note that a detailed derivation of equation 2.40 can be found in the appendix in section ?? and we have defined :

$$\begin{aligned} p &:= (p_1 p_2 - q_1 q_2) \\ q &:= (p_1 p_2 + q_1 q_2) \end{aligned} \tag{2.41}$$

For the identity of equation 2.40 we made use of Green's integration rule which allowed us to split the double integral to the product of two single integrations. Also, we used the definition of the 2-dimensional inverse Fourier transform of the height field function. We applied a similar substitution like we did in 2.35, but this time twice, once for x_1 and once for x_2 separately. The last step in equation 2.40, substituting with p and q in equation ?? will be useful later in the implementation. The insight should be, that the product of two complex numbers is again a complex number. We will have to compute the absolute value of $\mathcal{F}\{S\}(w_1, w_2)$ which will then be equal $(p^2 + q^2)^{\frac{1}{2}} \, |\mathcal{F}\{h\}(w_1, w_2)|$

2.6.2 Interpolation

In section 2.6.1 we derived an alternative approach to the gaussian window approach described in section 2.2.3 in order to approximate our height field. We assume that our height field is a superposition of periodically aligned substructured (i.e. finger structures). This so called PQ approach allows us to integrate over one period of a substructure in our height field, instead iterating over the whole domain. Nevertheless, this main finding, described in equation 2.40, is using the DTFT. Thus, since our original height field is supposed to be a continuous-time band-limited function we can reconstruct it by applying a sinc-interpolation.

In general, for a sinc-interpolation, we are interested in recovering an original analog signal $x(t)$ from its samples. Therefore, for a given sequence of real numbers $x[n]$, representing a digital signal, its correspond continuous function is:

$$x(t) = \sum_{n=-\infty}^{\infty} x[n] sinc\left(\frac{t - nT}{T}\right) \tag{2.42}$$

which has the Fourier transformation $X(f)$ whose non-zero values are confined to the region $|f| \leq \frac{1}{2T} = B$. When $x[n]$ represents time samples at interval T of a continuous function, then the quantity $f_s = \frac{1}{T}$ is known as its sample rate and $\frac{f_s}{2}$ denotes the Nyquist frequency. The sampling Theorem states that when a function has a Bandlimit B less than the Nyquist frequency, then $x(t)$ is a perfect reconstruction of the original function. Figure 2.6 illustrates a reconstruction of a 1d signal relying on a sinc-interpolation.

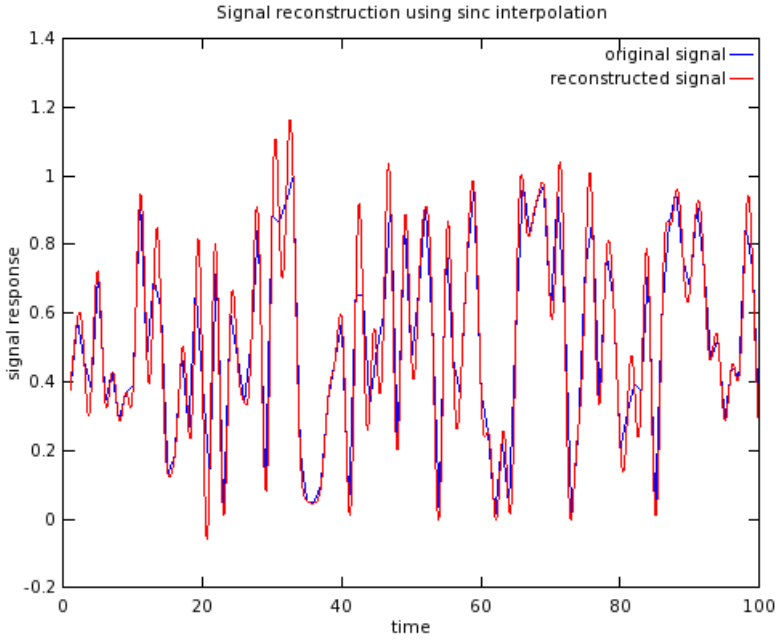

Figure 2.6: Comparison between a given random one dimensional input signal $s(t)$ and its sinc interpolation $\hat{s}(t)$. Notice that for the interpolation there were $N = 100$ samples from the original signal provided.

Bibliography

[Bar07] Bartsch, Hans-Jochen: *Taschenbuch Mathematischer Formeln*. 21th edition. HASNER, 2007. – ISBN 978–3–8348–1232–2

[CT12] Cuypers T., et a.: Reflectance Model for Diffraction. In: *ACM Trans. Graph. 31, 5* (2012), September

[DD14] D.S. Dhillon, et a.: Interactive Diffraction from Biological Nanostructures. In: *EUROGRAPHICS 2014/ M. Paulin and C. Dachsbacher* (2014), January

[D.S14] D.S.Dhillon, M.Single I.Gaponenko M.C. Milinkovitch M. J.Teyssier: Interactive Diffraction from Biological Nanostructures. In: *Submitted at Computer Graphics Forum* (2014)

[For11] Forster, Otto: *Analysis 3*. 6th edition. VIEWEG+TEUBNER, 2011. – ISBN 978–3–8348–1232–2

[I.N14] I.Newton: *Opticks, reprinted*. CreateSpace Independent Publishing Platform, 2014. – ISBN 978–1499151312

[JG04] Juan Guardado, NVIDIA: Simulating Diffraction. In: *GPU Gems* (2004). `https://developer.nvidia.com/content/gpu-gems-chapter-8-simulating-diffraction`

[LM95] Leonard Mandel, Emil W.: *Optical Coherence and Quantum Optics*. Cambridge University Press, 1995. – ISBN 978–0521417112

[MT10] Matin T.R., et a.: Correlating Nanostructures with Function: Structurral Colors on the Wings of a Malaysian Bee. (2010), August

[PAT09] Paul A. Tipler, Gene M.: *Physik für Wissenschaftler und Ingenieure*. 6th edition. Spektrum Verlag, 2009. – ISBN 978–3–8274–1945–3

[PS09] P. Shirley, S. M.: *Fundamentals of Computer Graphics*. 3rd edition. A K Peters, Ltd, 2009. – ISBN 978–1–56881–469–8

[R.H12] R.Hooke: *Micrographia, reprinted*. CreateSpace Independent Publishing Platform, 2012. – ISBN 978–1470079031

[RW11] R. Wright, et a.: *OpenGL SuperBible*. 5th edition. Addison-Wesley, 2011. – ISBN 978–0–32–171261–5

[Sta99] Stam, J.: Diffraction Shaders. In: *SIGGRPAH 99 Conference Proceedings* (1999), August

[T.Y07] T.Young: *A course of lectures on natural philosophy and the mechanical arts Volume 1 and 2*. Johnson, 1807, 1807